SC-RR-68-430

SC-RR-68-430

B-2

Fletcher

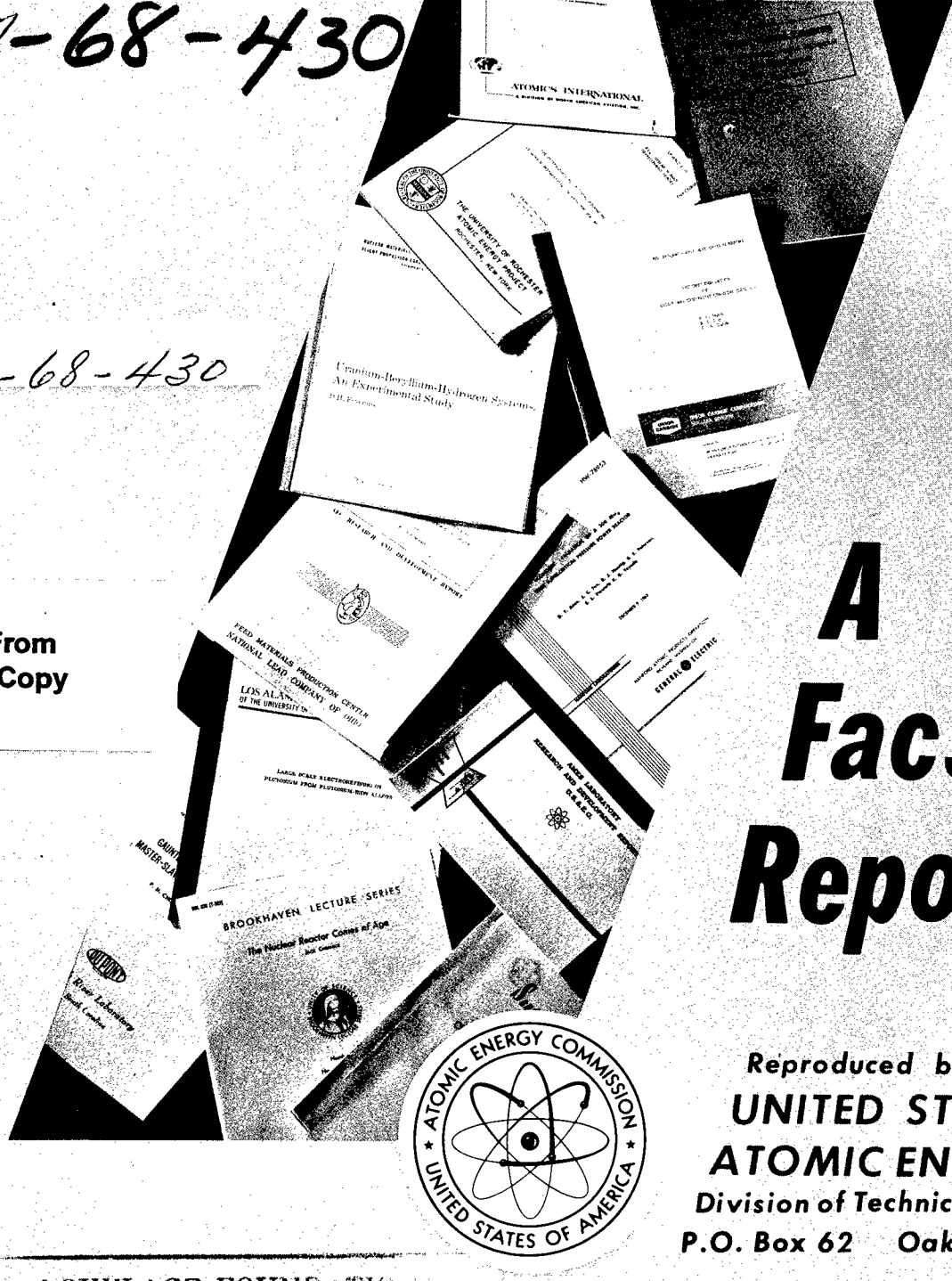

A Facsimile Report

Reproduced by
UNITED STATES
ATOMIC ENERGY COMMISSION
Division of Technical Information
P.O. Box 62 Oak Ridge, Tennessee 37830

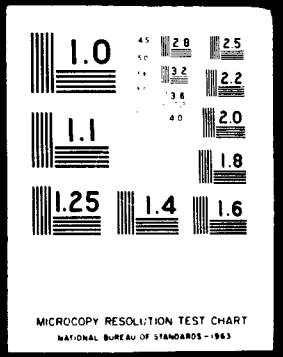

SC-RR-68-430

NUMERICAL RESULTS OF BLAST WAVE PROPAGATION IN TUNNEL INTERSECTIONS

L. D. Tyler, 9341
Sandia Laboratory
Albuquerque, New Mexico

September 1968

ABSTRACT

Blast wave diffraction and reflection are studied for a number of tunnel intersections. Transient pressure loading and resulting shock strengths after diffraction are determined by a finite difference technique.

kr

BLANK PAGE

ACKNOWLEDGMENT

The author wishes to acknowledge the efforts of Mr. J. H. Smith, 9424, in writing the TRANSHOK hydrodynamics code, and of Mr. W. D. Sundberg, 9341, in producing the computer plots of the results from TRANSHOK.

Printed in the United States of America
Available from
Clearinghouse for Federal Scientific and Technical Information
National Bureau of Standards, U. S. Department of Commerce
Springfield, Virginia 22151
Price: Printed Copy $3.00; Microfiche $0.65

CONTENTS

ILLUSTRATIONS

SYMBOLS

A	Coefficient for x "dissipative" term
B	Coefficient for y "dissipative" term
c	Speed of sound
e	Fluid particle energy
F	Column vector defined on page 12
f	Column vector defined on page 12
G	Column vector defined on page 12
K	Ratio of time increment to space increment, $\Delta t/\Delta x$
M_S	Shock Mach number
P	Pressure
t	Time
u	Velocity component in the x direction
v	Velocity component in the y direction
W	Tunnel width
x,y	Carestian coordinates
α	Coefficient of the "dissipative" difference term
γ	Specific heat ratio
η	Nondimensional time, tc_1/w
ρ	Density
σ	Courant number, $K\left\|(u^2 + v^2)^{1/2} + c\right\|$
φ	Difference "dissipative" function
ω	Dissipative parameter

Subscript

j	Mesh number for the x direction
k	Mesh number for the y direction
l	Reference to initial state of air

Superscript

n	Time mesh number

SUMMARY

This report gives a comparison of pressure loadings resulting from a blast wave for common types of intersections in an underground tunnel network. The intersections compared were the tee, cross, lateral tee, and elbow. Because of the transient nonlinear nature of the blast phenomenon in two dimensions, a finite-difference technique was used for the analysis.

The reflected pressure loadings in the intersection were compared with the maximum theoretical pressure for a normal reflection of the given blast wave. The elbow gave the most severe load; it peaked at 88 percent of the normal reflected value and decayed to 64 percent. The highest pressure for the tee intersection was 62 percent of the reflected value with a decrease to 54 percent. The lateral tee and cross intersections had the same results with maximum loads of 26 and 25 percent, respectively, which remained constant.

The comparison showed that the cross and lateral tee intersections experienced less pressure loading than the tee and elbow. The application of numerical techniques to this problem allowed a greater depth of analysis than would otherwise be possible.

NUMERICAL RESULTS OF BLAST WAVE PROPAGATION IN TUNNEL INTERSECTIONS

INTRODUCTION

In the past few years the primary method recommended for protecting people and equipment against enemy attack has been the establishment of underground shelters. In large underground systems a maze of corridors is required to connect the various parts of the overall network. In the design of such a network it may be important to consider the effect of tunnel intersections on the diffraction and reflection of a strong blast wave, because the design of these intersections determines the pressure loads on various parts of the network. Analysis of tunnel intersections has mainly been made on the basis of a one-dimensional transient method of characteristics for the blast wave and a wind resistance calculation which usually requires an experimental determination of overall system resistance factors. This approach has been used by Newman[1] in studying techniques for shock wave attenuation in tunnels and by Warren[2] for propagation of blasts along tunnels. Teel[3] has reported the experimental pressure histories for a number of simulated tunnel networks but did not measure pressures at the intersections. These studies give very useful results, but do not give the detailed local pressure loadings that may be needed by engineers in designing tunnel intersections and attenuation techniques such as baffles. The advanced development of numerical techniques and high-speed digital computers makes it possible for the engineer to perform to a greater depth the analysis of the diffraction and pressure loading of a blast wave. Therefore, a study of transient shock interaction and pressure histories in various tunnel intersection geometries has been conducted to aid in the design of underground protective shelters.

The tunnel intersection geometries studied are the tee, cross, lateral tee, and elbow. A comparison of these intersections is made on the basis of the resulting downstream blast wave, and the load history of the high-pressure locations. This comparison may be useful in eliminating undesirable intersections in the conceptual design of a tunnel network and in the determination of loadings for the structural design of intersections.

ANALYSIS

Governing Equations

Shock propagation in tunnel intersections is a transient, multi-dimensional phenomenon. The equations which govern such phenomena involve the conservation of mass, momentum, and energy, but neglect viscosity and conduction. The flow is assumed to be along a two-dimensional tunnel and to be plane with only two Cartesian spatial coordinates. The conservation equations are then written as

$$\frac{\partial f}{\partial t} + \frac{\partial F}{\partial x} + \frac{\partial G}{\partial y} = 0 \qquad (1)$$

where f, F, and G are the column vectors:

$$f = \begin{Bmatrix} \rho \\ \rho u \\ \rho v \\ e \end{Bmatrix} \; ; \quad F = \begin{Bmatrix} \rho u \\ \rho u^2 + p \\ \rho uv \\ (e + p)u \end{Bmatrix} \; ; \quad G = \begin{Bmatrix} \rho v \\ \rho uv \\ \rho v^2 + p \\ (e + p)v \end{Bmatrix} .$$

The gas is assumed to be perfect and obeys the equation of state

$$e = \frac{p}{\gamma - 1} + \frac{\rho(u^2 + v^2)}{2} \qquad (2)$$

The governing system of equations is quite complex, with Equation 1 being a set of four quasilinear partial differential equations and Equation 2 being a non-linear algebraic equation. Therefore, the equations are solved using a finite difference technique. The governing equations are said to be in conservation form and describe only reversible flow processes. Because of the presence of shock waves, a method of accounting for their propagation and diffraction must be used. Therefore, a smoothing or artificial "dissipative" function is included in the finite difference technique. The dissipative function used here has the form

$$\frac{\partial}{\partial x}\left|A\frac{\partial f}{\partial x}\right| + \frac{\partial}{\partial y}\left|B\frac{\partial f}{\partial y}\right|$$

and is added to the right side of Equation 1.

The effect of this "dissipative" function is to cause the shock transition to be a smooth one extending over a small number of space difference intervals and to influence the stability of the finite difference solution. A discussion of the mathematical properties and the use of "dissipative" functions is given by the author in Reference 4. The "dissipative" technique used was first presented in difference form by V. V. Rusanov[5] and was later studied by the author and G. W. Zumwalt[6].

Difference Equations

Using a forward difference for the time derivative, and centered differences for the space derivatives, the difference equations for a general point (j, k), where j and k correspond to the x and y directions, respectively, at time n is given as

$$f^{n+1}_{j,k} = f^{n}_{j,k} - \frac{K}{2}\left\{F_{j+1,\,k} - F_{j-1,\,k} + G_{j,\,k+1} - G_{j,\,k-1}\right\}^{n} + 1/2\left\{\varphi_{j+1/2,\,k} - \varphi_{j-1/2,\,k} + \varphi_{j,\,k+1/2} - \varphi_{j,\,k-1/2}\right\}^{n} \qquad (3)$$

where

$$\varphi^{n}_{j+1/2,\,k} = \alpha^{n}_{j+1/2,\,k}\left[f_{j+1,\,k} - f_{j,\,k}\right]^{n} ,$$

$$\varphi^{n}_{j-1/2,\,k} = \alpha^{n}_{j-1/2,\,k}\left[f_{j,\,k} - f_{j-1,\,k}\right]^{n} ,$$

$$\alpha^{n}_{j+1/2,\,k} = \frac{\left(\sigma_{j+1,\,k} + \sigma_{j,\,k}\right)^{n}}{2} ,$$

and

$$K = \Delta t/\Delta x = \Delta t/\Delta y$$

$$\alpha^{n}_{j,\,k} = 2\,\frac{\Delta t}{(\Delta x)^2}\,A^{n}_{j,\,k} = 2\,\frac{\Delta t}{(\Delta y)^2}\,B^{n}_{j,\,k}$$

The relations for φ and α may be applied to the k direction by interchanging the roles of j and k. The φ terms represent the artificial "dissipative" function. From a Fourier stability analysis the relation-

ship for $\alpha^n_{j,\,k}$ becomes

$$\alpha^n_{j,\,k} = \frac{\omega\sigma^n_{j,\,k}}{2} \tag{4}$$

where

$$\sigma^n_{j,\,k} = K\left[\left(u^2 + v^2\right)^{1/2} + c\right]^n_{j,\,k} ,$$

c = sonic velocity

ω = dissipative parameter

and the stability conditions are

$$\left(\sigma^n_{j,\,k}\right)^2 \le \omega\sigma^n_{j,\,k} \le 1 \quad . \tag{5}$$

Boundary Conditions

The boundary conditions used for a solid surface are satisfied by using the reflection principle.[7,8] Values of the dependent variables are assigned to a virtual point defined inside the body and used in the difference equation.

A detailed discussion of the development and advantages of using the reflection principle is given by W. F. Walker and G. W. Zumwalt[8]. The reflection principle is demonstrated by considering a solid boundary as shown in Figure 1. The variables at the field point (j, k+1) would be related to the variables at the virtual point (j, k-1) by the expressions

$$\rho_{j,\,k+1} = \rho_{j,\,k-1}$$

$$u_{j,\,k+1} = u_{j,\,k-1}$$

$$v_{j,\,k+1} = -v_{j,\,k-1}$$

$$p_{j,\,k+1} = p_{j,\,k-1}$$

$$\varphi_{j,\,k+1} = \varphi_{j,\,k-1}$$

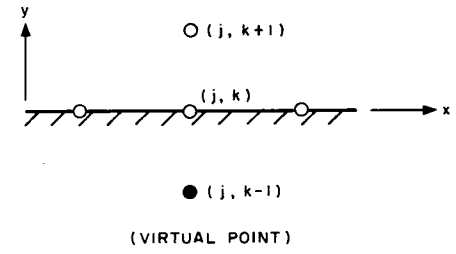

Figure 1. Reflection Principle for a Wall Point

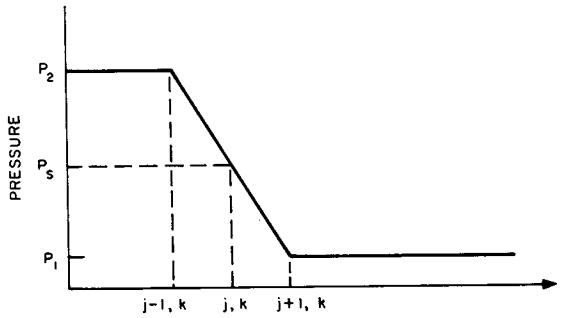

Figure 2. Initial Shock Pressure Distribution

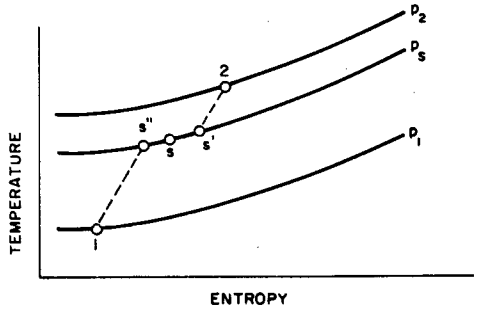

Figure 3. Temperature Entropy Diagram for Initial Shock Conditions

The smoothing terms acting in a direction normal to the wall are eliminated so as to reduce the artificial "dissipation" normal to the wall. For a solid boundary parallel to the y axis, the image point relations are

$$\rho_{j+1,\,k} = \rho_{j-1,\,k}$$

$$u_{j+1,\,k} = -u_{j-1,\,k}$$

$$v_{j+1,\,k} = v_{j-1,\,k}$$

$$p_{j+1,\,k} = p_{j-1,\,k}$$

$$\varepsilon_{j+1,\,k} = \varepsilon_{j-1,\,k}$$

One important advantage of the reflection boundary principle is that it allows boundary points to be treated by centered difference. Therefore, the general field difference Equation 3 may be used at solid boundary points.

Initial Conditions

The initial conditions are given by establishing a shock wave at some position upstream of the tunnel intersection. Because a mathematical "dissipative" technique is used, the shock wave is blurred over a few difference increments. Therefore, the initial shock profile is defined over two space increments, as shown in Figure 2, to decrease initial disturbance in the computation. The temperature-entropy diagram of Figure 3 may be used to describe the method of determining the conditions of state s at the center of the shock. The pressure at the shock center, p_s, is the arithmetic mean of the pressure in front of and behind the wave. Intermediate shock waves are assumed to exist from states 1 to s' and s" to 2. This allows the velocity and density at s' and s" to be determined. The values of density and velocity at state s are then given by the arithmetic mean of the respective values at s' and s". Details of this initial condition method for moving shock waves are given by the author and G. W. Zumwalt[9].

The finite-difference technique described has been included in the Sandia Laboratory hydrodynamic computer code TRANSHOK for transient shock propagation.

RESULTS

Input Conditions

The incident shock wave has the same initial conditions (Table I) for all the examined intersection geometries. The flow properties are referred to the initial state of the undisturbed air before shock passage. The initial state of the air is denoted by the subscript 1.

Table I

Initial Shock Wave Conditions

Mach No.	$M_s = 23.91$
Pressure ratio	$P/P_1 = 666.67$
Density ratio	$\rho/\rho_1 = 5.948$

The position and propagation direction of the shock wave at time zero, and the dimensions of the computing mesh, are shown in Figure 4 for the four intersection geometries. The initial shock wave is defined at the first two mesh columns of the computation field for all geometries. The tunnel width, W, is 10 mesh increments for both the incident and the lateral tunnels in all cases. The results of the transient shock computations in these geometries are given in the form of computer plots of the velocity vector and pressure topology fields for various nondimensional times, η, where η equals tc_1/W. The nondimensional time, η, may be better understood by considering a blast wave propagating in a 10-foot wide tunnel into an atmosphere having a sound speed of 1100 ft/sec. The nondimensional time, η of 0.1 under these conditions equals 0.909 milliseconds. Because of the flow symmetry about the incident tunnel centerline, only half a plane of results is shown of the pressure topology for the tee and cross tunnel intersections.

Tee Intersection

The tee geometry (Figure 4-a) allows the shock wave to propagate along the incident passage and be divided at the intersections into two

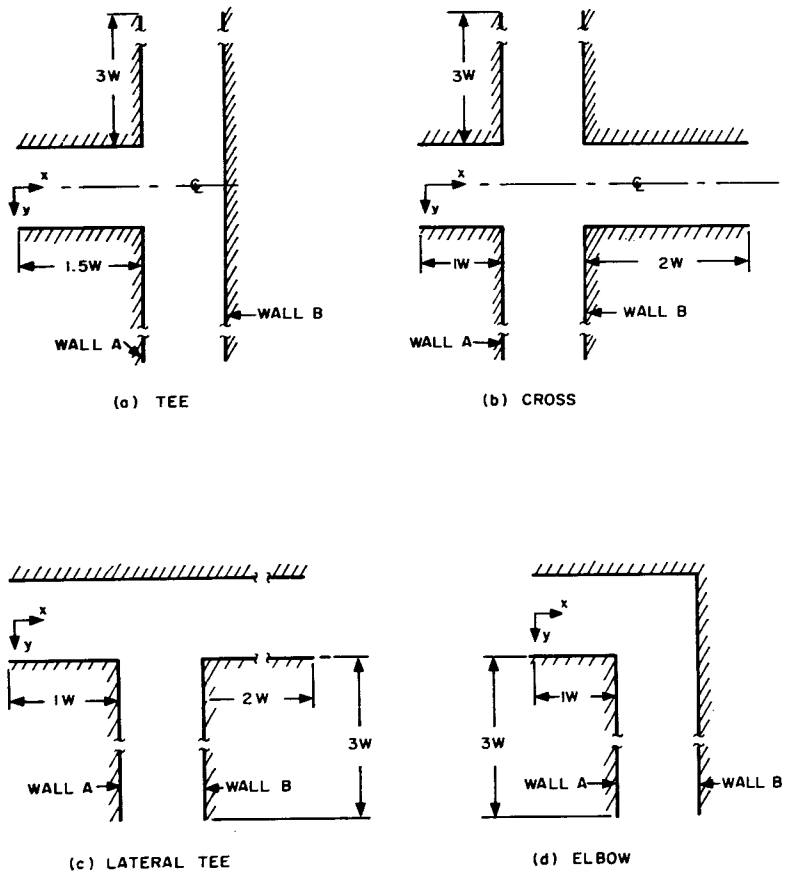

Figure 4. Tunnel Intersection Geometries

shock waves of equal strength which reverberate along the lateral tunnels. By inspecting the velocity and pressure results in Figure 5, the shock wave at $\eta = 0.058$ is observed to be diffracting around the intersection corners and moving into the lateral tunnels. The shock wave continues to move along Wall A, and at $\eta = 0.116$ has reflected from Wall B, causing a large concentrated pressure loading in the vicinity of the intersection of the incident tunnel centerline and Wall B. Also, at this time the flow is quite nonuniform and is directed towards Wall B. The shock wave has been reflected from Wall B at $\eta = 0.173$ and is moving toward Wall A with a pressure ratio that is reduced from its original value. At $\eta = 0.230$ the shock has reflected from Wall A and is approximately 3.5 W from the incident tunnel centerline, and the shock pressure ratio, P/P_1, varies from 620 on Wall A to 330 on Wall B. The highest pressure loading occurring in this flow is a stagnation point resulting from the initial reflection of the shock wave on Wall B. The pressure history of this point is shown in Figure 6. The pressure reaches a maximum value of $P/P_1 = 3315$, which is applied only for a short time and then decreases to a value of 2890. The reflected pressure at the high pressure point is 62 percent of the maximum theoretical pressure, $P/P_1 = 5340$, given for the normal reflection of a shock wave having the same strength.

Cross Intersection

A shock wave which interacts with the cross-geometry intersection (Figure 4-b) is divided into three shock waves: two shock waves of equal strength which propagate into the lateral tunnels, and a shock which continues to move along the centerline. The velocity and pressure fields in Figure 7 show that the initial shock wave has begun to diffract into the lateral tunnels at $\eta = 0.0579$. A short time later, at $\eta = 0.115$, the initial shock has been divided into three waves, with two waves being reflected from Wall B and a uniform wave moving downstream along the centerline. The centerline shock has a pressure ratio P/P_1, of 560 which is a 16 percent reduction from the incident pressure ratio of 666.67. The shock waves in the lateral tunnels are reflected from the downstream corners on Wall B, causing a high pressure loading. At $\eta = 0.172$ the reflected waves in the lateral tunnels are moving toward Wall A and the centerline shock wave has passed out of the computation field, leaving a uniform flow in the centerline tunnel. In the lateral tunnels at $\eta = 0.228$ the shock has reflected from Wall A. The shock is approximately 3 W from the incident tunnel centerline at this time and

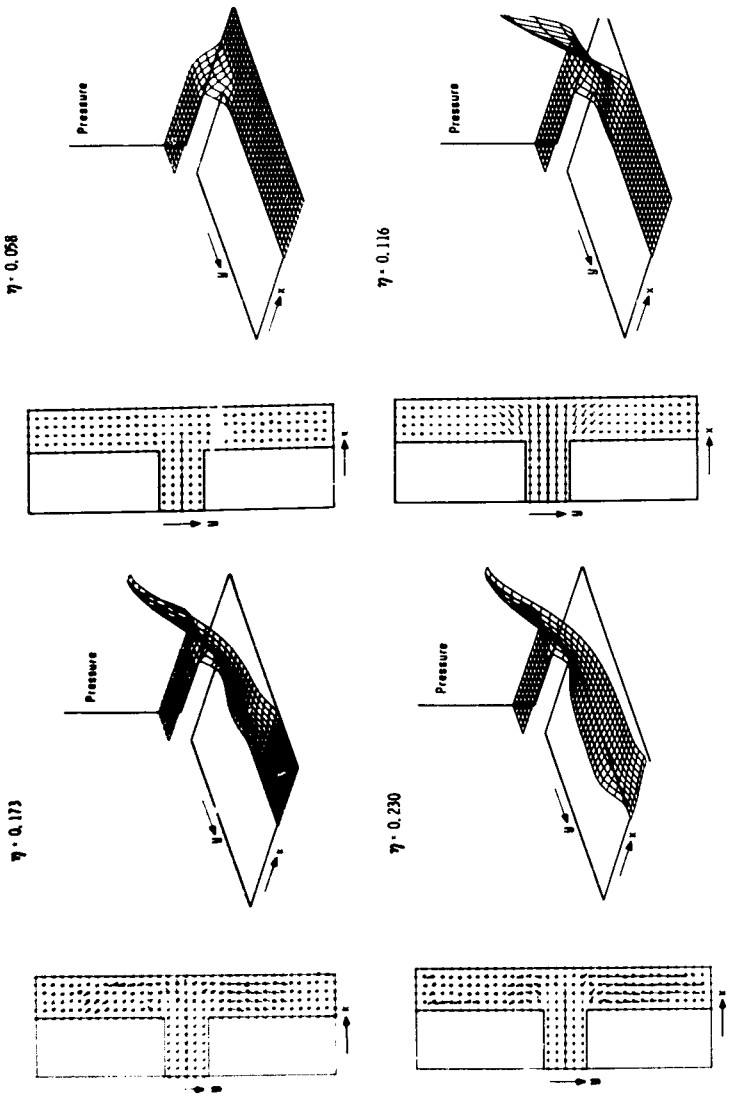

Figure 5. Time Sequence of Velocity and Pressure Topology Fields for the Tee Intersection

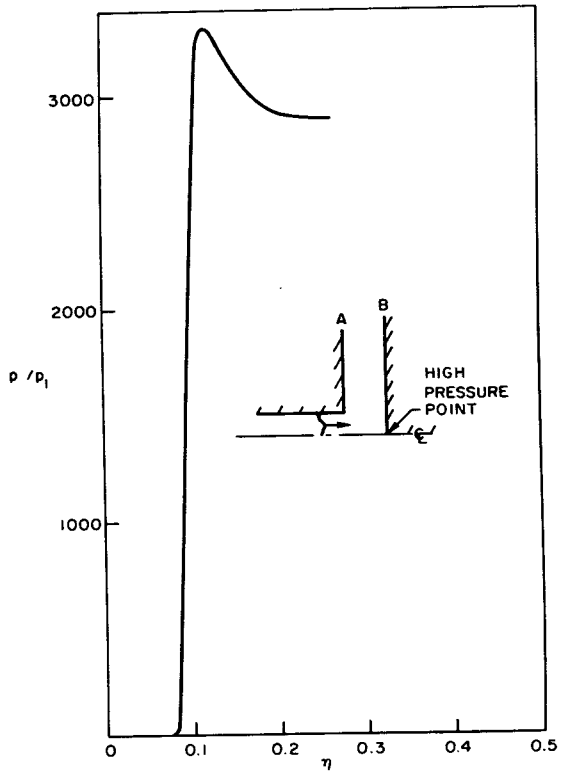

Figure 6. Pressure History of the Point of Highest Load in the Tee Intersection

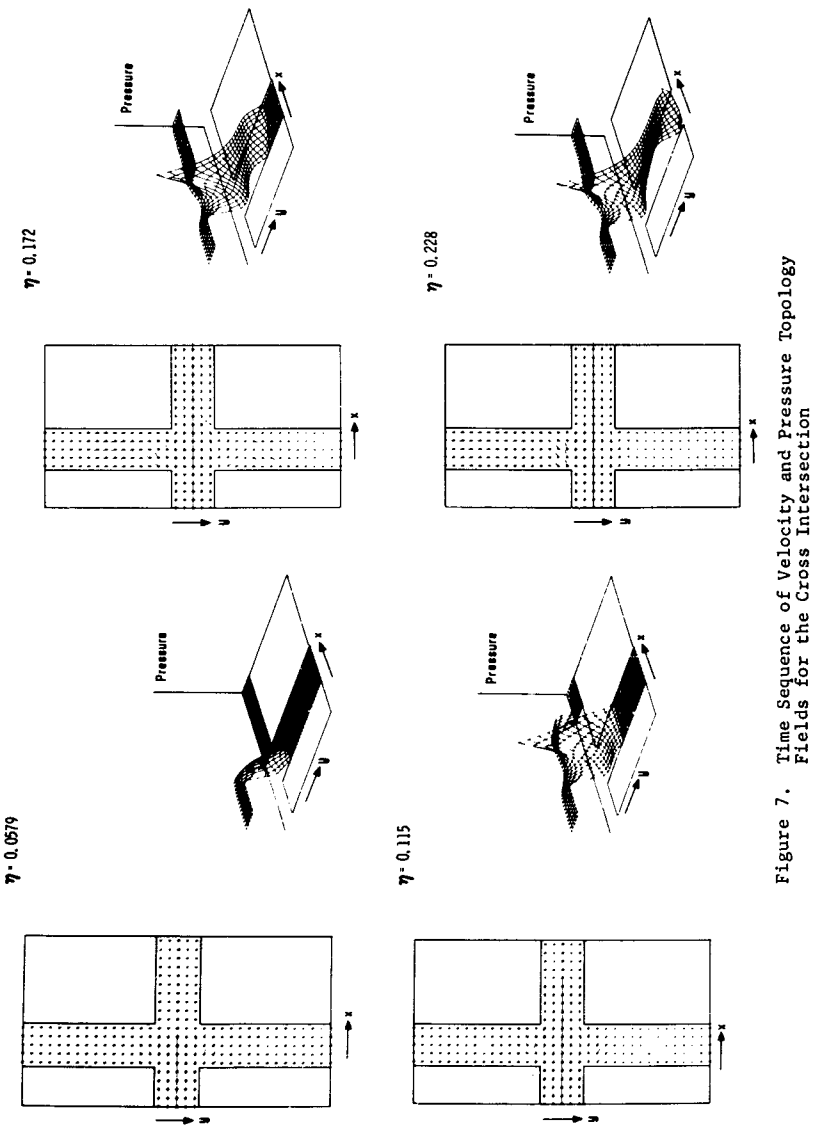

Figure 7. Time Sequence of Velocity and Pressure Topology Fields for the Cross Intersection

has a pressure ratio which varies across the tunnel from 305 on Wall A to 195 on Wall B. A comparison of the pressure fields at $\eta = 0.172$ and 0.228 shows the flow to be approximately steady state at the intersection. The downstream corners on Wall B are the high pressure points in this flow geometry. The pressure history of these points is shown in Figure 8 where the maximum pressure obtained is 1345 and decreases to 1325.

Lateral Tee Intersection

The flow in the lateral tee tunnel intersection is very similar to that in the cross intersection except that the incident shock is divided into two waves because there is only one lateral tunnel. This point is borne out by inspection of the velocity and pressure results of Figure 9. The incident wave begins to diffract into the lateral tunnel at $\eta = 0.058$. At a later time ($\eta = 0.115$) two shocks are propagating away from the intersection. The shock wave moving along the downstream extension of the incident tunnel is uniform and has a pressure ratio (P/P_1) of 610, which is about a 9 percent decrease in strength from the initial shock. The shock wave in the lateral tunnel at this time has reflected from the downstream corner on Wall B and is moving toward Wall A. The lateral tunnel shock at $\eta = 0.172$ has reflected from Wall A and propagates toward Wall B. Finally, when the wave is 3 W from the intersection at $\eta = 0.229$, the pressure ratio varies from 331 on Wall B to 185 on Wall A. It should be noted that the flow is fairly steady at the tunnel intersection by this time. The location of the high pressure point for this intersection is the same as that for the cross intersection: at the downstream corner on Wall B. The pressure history at this point, as shown in Figure 10, rises to a maximum value of 1396 and then decreases to 1385.

Elbow Intersection

The elbow tunnel intersection represents a case in which the initial shock wave is not divided, but is simply diverted in a 90-degree turn. The velocity and pressure fields of Figure 11 show that at $\eta = 0.057$ the wave has begun to diffract around the bend. At $\eta = 0.114$ the shock has reflected from Wall B and is directed toward Wall A. At the later times $\eta = 0.173$ and 0.228, the shock reflects between Walls A and B. At $\eta = 0.228$ the shock is about 3 W from the bend and the pressure ratio varies from 750 on Wall A to 580 on Wall B. The location of the highest pressure is at the corner between Wall B and the incident tunnel wall.

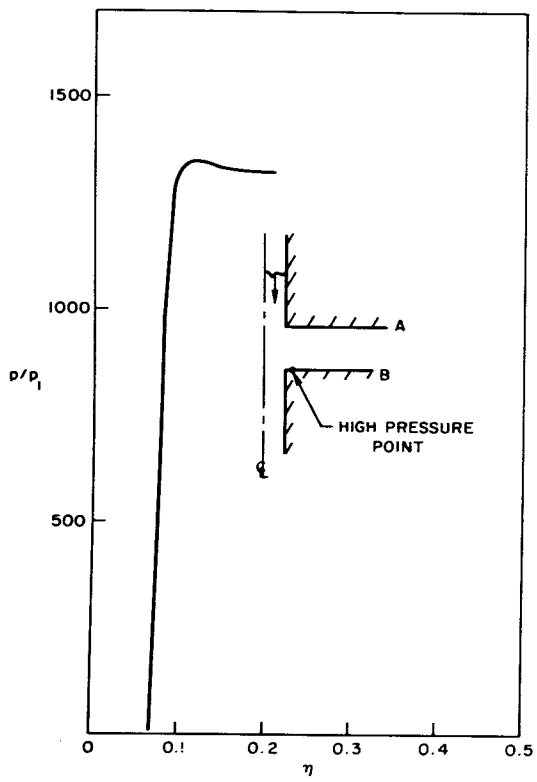

Figure 8. Pressure History of the Point of Highest Pressure in the Cross Intersection

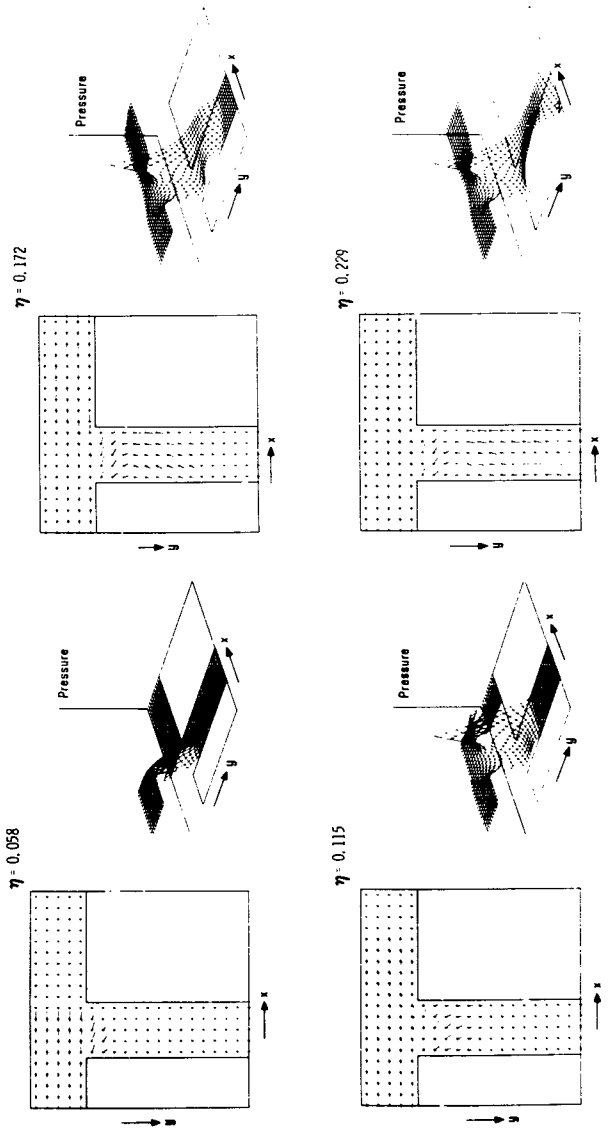

Figure 9. Time Sequence of Velocity and Pressure Topology Fields for the Lateral Tee Intersection

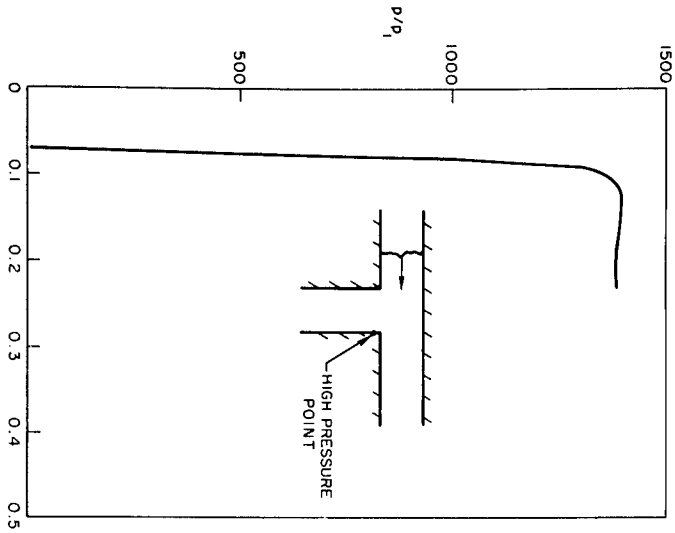

Figure 10. Pressure History of the Point of Highest Load in the Lateral Tee Intersection

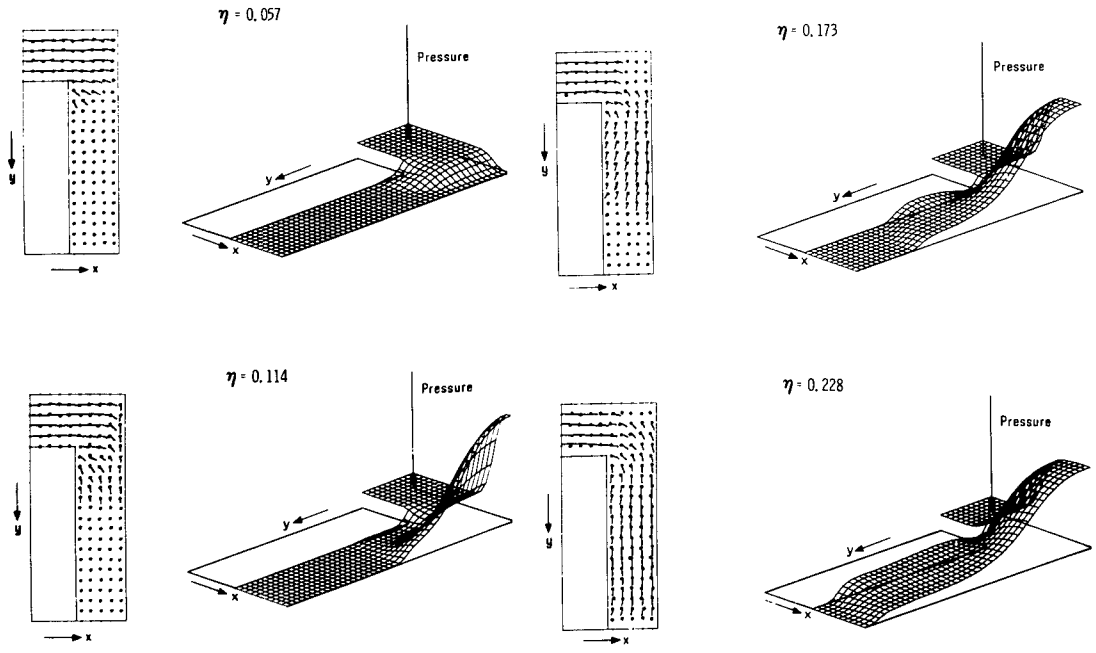

Figure 11. Time Sequence of Velocity and Pressure Topology Fields for the Elbow Intersection

Figure 12 shows that the pressure at this location increased to 4710, which is about 89 percent of the maximum possible theoretical reflected pressure ratio. The pressure decays quite rapidly to a resulting pressure ratio below 3400, which is still 64% of the theoretical maximum reflected pressure ratio.

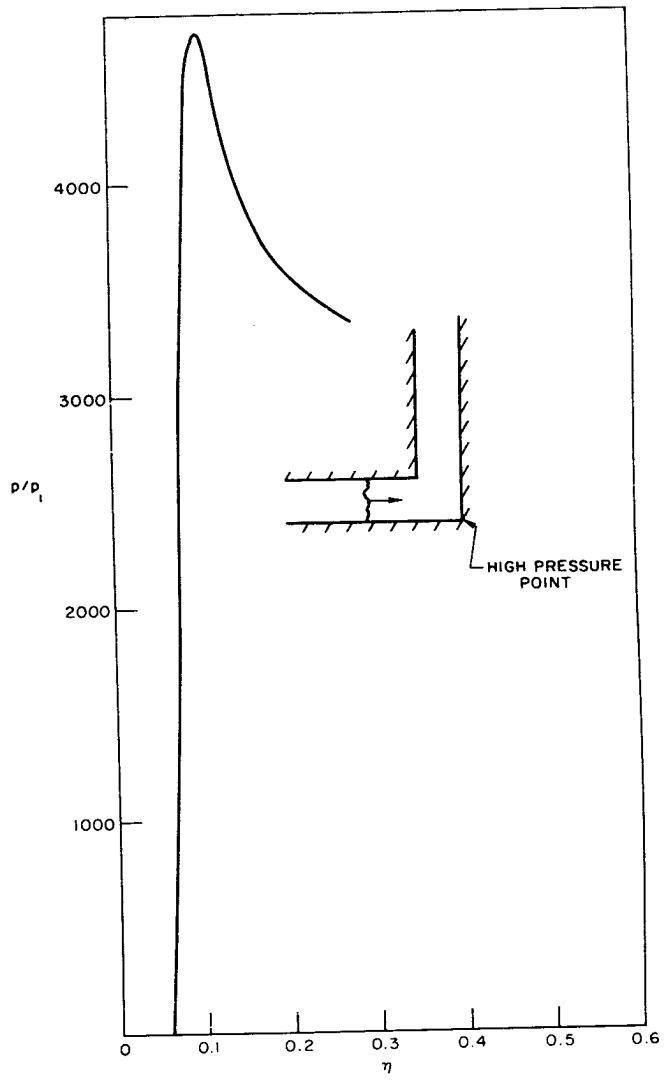

Figure 12. Pressure History of the Point of Highest Load in the Elbow Intersection

DISCUSSION

To compare the effect of a blast wave on the above tunnel intersections, the strength of the resulting shock waves in the downstream tunnels and the pressure history of the high load points should be examined. The pressure ratios (P/P_1) behind the shock waves in the downstream tunnels are given in Table II. The shock wave conditions in the lateral tunnels are given for the time when the wave is approximately 3 W from the intersection centerline. For the nonuniform shock waves, an average pressure ratio is used for comparison purposes. Also given in Table II is the percentage comparison of the average downstream shock strength to the initial shock strength.

Table II

Downstream Shock Wave Pressure Ratio P/P_1

Configuration	Wall A	Wall B	Lateral Tunnel Avg.	Lateral Tunnel %	Downstream Tunnel Avg.	Downstream Tunnel %
Tee	620	330	475	72		
Cross	305	195	250	38	560	84
Lateral Tee	185	331	258	39	610	91
Elbow	750	580	665	100		

The cross and lateral tee intersections have strong shocks in the downstream tunnels, and waves which are about 60 percent weaker in the lateral tunnels. The tee intersection divides the incident blast wave into two waves, with the shock strength reduced by 28 percent. The elbow gives no reduction in shock strength. In addition to the strength of the resulting shock waves produced in these intersections, the pressure history for the high load points is shown in Figure 13. Also shown in Figure 13, for reference, is the maximum theoretical pressure ratio that a shock wave of strength 666.67 could attain for a normal reflection on a plane wall. The elbow intersection is the most severe case, with a pressure loading considerably higher than the other three cases. The elbow peak pressure initially is 88 percent of the reference

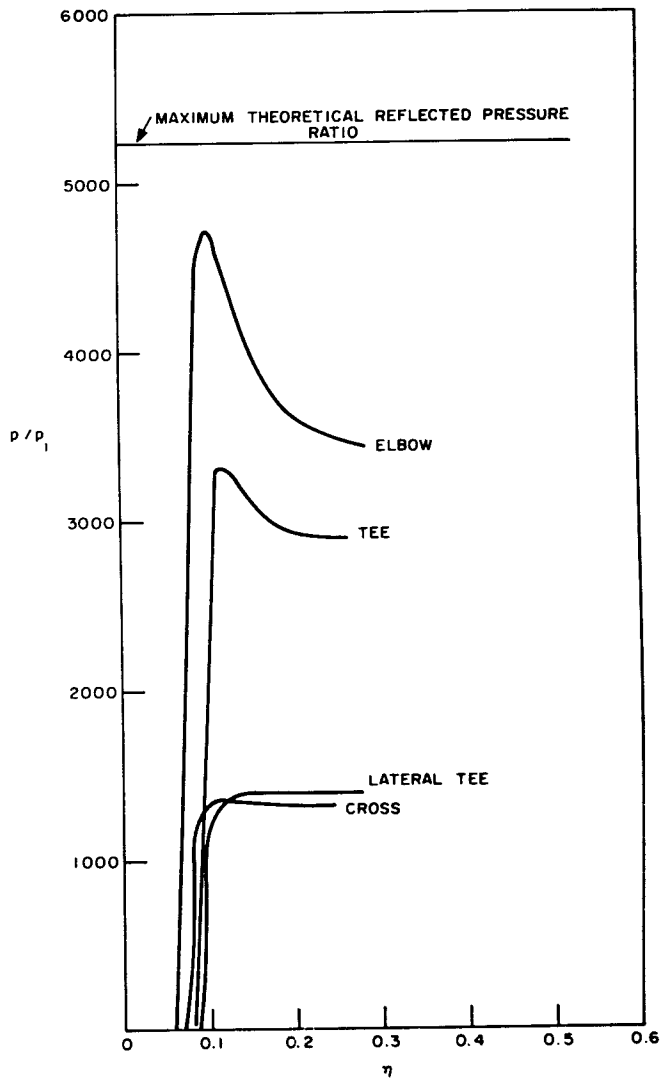

Figure 13. Comparison of the Pressure Histories of the Highest Load Points for All Intersections

pressure, decaying to about 64 percent of the reference. The tee peak pressure is 62 percent with a reduction to 54 percent. Both the cross and lateral tee intersections have high pressure loads which are only 25 percent of the reference with no decay, and are less than half the maximum pressures found in tee and elbow intersections.

CONCLUSIONS

The analysis of the blast wave effects on the four tunnel intersections shows that the elbow and tee tunnel intersections experience much higher pressure loadings than the cross and lateral tee configurations. It is shown that configurations in which a nearly normal shock reflection can occur should be avoided if possible.

When a tee intersection is used, the resulting downstream shock strengths are only about 25 percent of the initial base wave strength. The cross and lateral tee tunnel intersections are the most desirable because of the low pressure loadings and the weaker shock waves in the lateral tunnels.

It should also be noted that the utilization of numerical techniques can be very helpful in establishing the shock loads for designing tunnel complexes.

REFERENCES

1. Newman, J., Attenuation of Shock Waves in Tunnel Shelters, Oak Ridge National Lab., Tech. Memo., ORNL - TM-1622, Sept. 1966.

2. Warren, A., Propagation of Blast Waves Along Tunnels (U), Armament Research and Development Establishment Report, ARDE Report (MX) 27/58, Confidential, Nov. 1958.

3. Teel, G. D., Blast Patterns in Complex Tunnel Models, Ballistic Research Lab., BRL-TN-1533, Apr. 1964.

4. Tyler, L. D., Mathematical Conservation Laws Applied to Gas Dynamics, Sandia Lab Tech. Memo., SC-TM-66-10, 1966.

5. Rusanov, V. V., "The Calculation of the Interaction of Non-Stationary Shock Waves and Obstacles," National Research Council of Canada Library, Ottawa, Canada, Tech. Translation 1027 by D. A. Sinclair, 1962. Translated From: Zhurnal Vychislitelnoi Fiziki, (Akademiya Nauk), SSR 1, Vol. 1, No. 2, 1961, p. 267.

6. Tyler, L. D., and Zumwalt, G. W., "Numerical Solution of the Flow Field Produced by a Shock Wave Emerging into a Crossflow," Heat Transfer and Fluid Mechanics Institute, Santa Clara, Calif., 1966.

7. Walker, W. F. and Zumwalt, G. W., A Numerical Solution for the Interaction of a Moving Shock Wave with a Turbulent Mixing Region, Sandia Lab Rept., SC-CR-67-2531, 1966.

8. Burstein, S. Z., "Numerical Methods in Multidimensional Shocked Flows," AIAA Journal, Vol. 2, No. 2, 1964, p. 2111.

9. Tyler, L. D. and Zumwalt, G. W., Numerical Solutions of the Flow Field Produced by a Plane Shock Wave Emerging Into a Crossflow, Sandia Lab Rept., SC-DC-65-1916, 1965.

END

DATE FILMED

8/11/70